A small field of view camera for hybrid gamma and optical imaging

2014 JINST 9 C12020

(http://iopscience.iop.org/1748-0221/9/12/C12020)

PUBLISHED BY IOP PUBLISHING FOR SISSA MEDIALAB

RECEIVED: *September 23, 2014*
ACCEPTED: *October 28, 2014*
PUBLISHED: *December 10, 2014*

10th INTERNATIONAL CONFERENCE ON POSITION SENSITIVE DETECTORS
7–12 SEPTEMBER 2014,
UNIVERSITY OF SURREY, GUILDFORD, SURREY, U.K.

A small field of view camera for hybrid gamma and optical imaging

J.E. Lees,[a,1] **S.L. Bugby,**[a] **B.S. Bhatia,**[a] **L.K. Jambi,**[a] **M.S. Alqahtani,**[a] **W.R. McKnight,**[a] **A.H. Ng**[b] **and A.C. Perkins**[b]

[a] *Space Research Centre, Michael Atiyah Building, University of Leicester, Leicester, LE1 7RH, U.K.*

[b] *Radiological and Imaging Sciences, Medical School, University of Nottingham, Nottingham, NG7 2UH, U.K.*

E-mail: John.Lees@leicester.ac.uk

ABSTRACT: The development of compact low profile gamma-ray detectors has allowed the production of small field of view, hand held imaging devices for use at the patient bedside and in operating theatres. The combination of an optical and a gamma camera, in a co-aligned configuration, offers high spatial resolution multi-modal imaging giving a superimposed scintigraphic and optical image. This innovative introduction of hybrid imaging offers new possibilities for assisting surgeons in localising the site of uptake in procedures such as sentinel node detection. Recent improvements to the camera system along with results of phantom and clinical imaging are reported.

KEYWORDS: Gamma camera, SPECT, PET PET/CT, coronary CT angiography (CTA); Multi-modality systems; Intra-operative probes

[1] Corresponding author.

doi:10.1088/1748-0221/9/12/C12020

Contents

2014 JINST 9 C12020

1 Introduction

Nuclear medical images are typically acquired using large field of view (LFOV) gamma cameras designed for whole body scanning and SPECT imaging. However, a new generation of small field of view (SFOV) gamma cameras, now in development, has been designed to provide higher resolution capabilities for specific procedures, such as sentinel node localisation.

A number of researchers and manufacturers have been developing a range of small hand-held or portable systems for medical gamma imaging [1–10]. These smaller systems have all concentrated on a single imaging modality. This communication describes a compact dual-modality camera that combines optical and gamma ray imaging into a single system. We also report on a number of studies using thyroid and lymphatic phantoms and a recent clinical image showing the benefit of a combined optical and gamma image.

2 Compact Gamma Camera

The Compact Gamma Camera (CGC) combines an optical and a gamma camera in a configuration that offers high spatial resolution multi-modality imaging with the option for a fused image output. The basic design is flexible with a range of collimators that can be selected to balance the requirements of spatial resolution and sensitivity to match to a wide variety of applications.

The CGC consists of a charge-coupled device (CCD), a CsI(Tl) scintillator coupled to the CCD (e2v CCD97 BI [11]) and a tungsten pinhole collimator. The CCD to pinhole distance is fixed at 10 mm. The distance from the pinhole to the object under examination determines the magnification of the system. Gamma-ray photons arriving from the source will interact with the

scintillator and generate optical photons, the number being related to the absorbed photon energy, which are subsequently detected by the CCD — allowing the position and the energy of the incident gamma photon to be recorded [2]. The hybrid camera head is surrounded by tungsten shielding (3 mm thickness) and sealed in a non-toxic plastic enclosure to provide both thermal and electrical isolation. Figure 1 shows the CGC being operated in a hand held mode.

Figure 1. Photograph of the CGC being used in a clinical setting.

Figure 2 (l.h.s.) shows a simplified schematic of the hybrid system; the hybrid camera head comprises of the standard CGC, a thin (3 mm thickness) first surface mirror at 45 degrees and an optical camera outside the direct line of sight of the pinhole. A photograph of the optical mount is also shown (r.h.s.).

In an early version of the hybrid system [2] the optical camera was positioned directly in front of the gamma camera. A low cost webcam with a precision pinhole (100 μm diameter) was used to obtain the optical image. Although this design was simple to implement, it had a number of disadvantages — most significantly the absorption of a portion of the gamma rays by the electronics located on the back of the camera. In the updated configuration (see figure 2), gamma photons from the source will pass through the mirror with minimal absorption ($< 3\%$) and scatter, whereas the optical photons are reflected towards the optical camera. Both the optical and gamma cameras are connected to a readout and control electronics system managed by a PC.

The CGC has been designed to be sensitive over the energy range 30–140 keV. At present, the CGC uses a Hamamatsu [12] CsI(Tl) columnar scintillator (600 μm thick on an amorphous carbon substrate) coupled directly to the CCD with Dow Corning optical grease. This thickness of scintillator has an absorption ranging from $\sim 100\%$ to 20% over the energy range of interest [2].

The CGC uses a single pinhole collimator, partly to simplify the construction but also to extend the imaging field of view which, for a parallel-hole collimator, would be limited to the image area of the CCD (~ 8 mm $\times$ 8 mm [2]). Two collimators were manufactured [13] from tungsten discs, 6 mm thick and 45 mm in diameter with pinholes of 0.5 mm or 1.0 mm diameter, both having an acceptance angle of 60 degrees. The transmission through 6 mm thick tungsten is $< 4 \times 10^{-9}$ at 140 keV, thereby limiting detected gamma rays to those passing through the pinhole.

2014 JINST 9 C12020

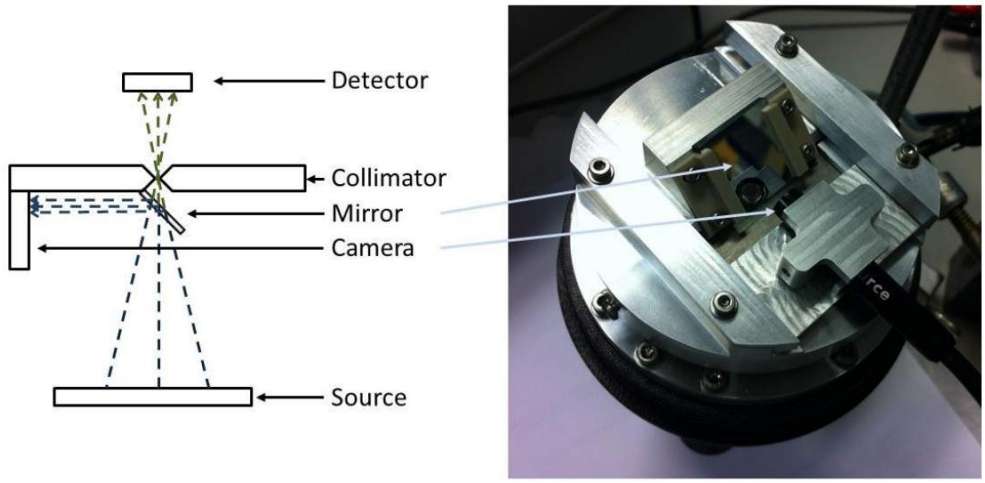

Figure 2. L.h.s. shows a schematic of the hybrid CGC system. An optical mirror is located in front of the collimator of the CGC with the optical camera positioned to one side. R.h.s. a photograph of the optical assembly located on top of the gamma camera head.

There are a number of factors that determine the sensitivity of gamma cameras that use pinhole collimators including photon energy, collimator material, pinhole diameter and acceptance angle. For a point-like object at 25 mm, the on-axis geometric sensitivities were estimated to be 4.3×10^{-5} and 1.4×10^{-4} (with 0.5 mm and 1.0 mm diameter pinholes respectively) for 140 keV gamma photons.

2.1 Imaging software

The system can operate in either single- or dual-modality mode. Each image format can be displayed independently or in a fused co-aligned image with adjustable contrast and colour tables to help interpretation.

A full gamma image consists of many individual frames acquired over a period of time, typically ranging from 100–20,000 frames. The image is analysed on a frame by frame basis using a "blob-detection" algorithm with automatic scale selection [2]. This analysis approach gives information on the number and intensity of all gamma interactions within the scintillator, which in turn gives information on the energy distribution of the gamma events. The optical images are captured directly from the optical camera electronics using bespoke interface software which allows for the capture of images from multiple cameras. Each image is imported directly into the main acquisition software for display and analysis. The current optical cameras are simple webcams chosen for their low profile, low cost and availability.

3 Modelling

A new Monte Carlo model, independently developed in IDL,[1] has been specifically designed to simulate the response of a pinhole-collimated scintillator-based gamma camera to incident photons. This model was developed to allow greater flexibility in both input and output information than a

[1] IDL, Interactive Data Language, Exelis Visual Information Solutions RG12, 1WA, U.K.

2014 JINST 9 C12020

proprietary software package. The aim of its development was to fully understand the responses of components of the CGC.

3.1 Scope of model

The model simulates gamma photon attenuation from photoelectric absorption, Compton and Rayleigh scattering along with fluorescence and Auger transitions. Within the scintillator, energy deposition and transport (including reflection effects) are modelled. A simulated image is formed based upon the detection of scintillation photons in the CCD, along with the modelled effects of noise from the CCD and associated electronics. Final results may be viewed in real time or recorded for further analysis.

3.2 Modelling results

The model allows for the investigation of response from individual camera components along with the device as a whole. The model has been used to investigate sensitivity, spatial resolution and energy resolution and shows a good agreement with theoretical and experimental values. Figure 3 shows an example simulated image and an experimental image acquired with the CGC under similar conditions. A full description of the model will be reported in a future paper. We anticipate that the simulation will be used to guide future developments of the CGC.

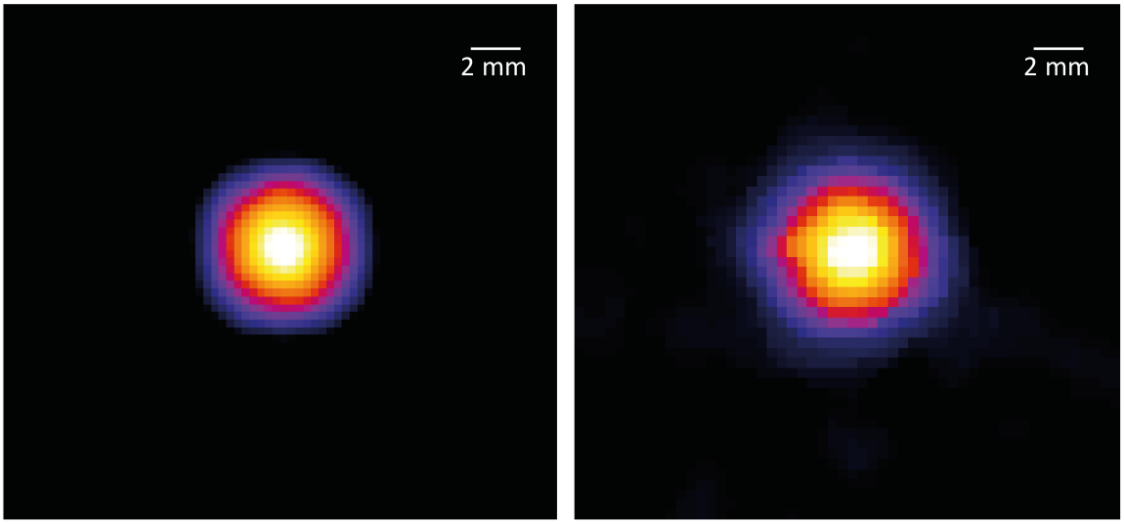

Figure 3. Left: modelled hot spot. Right: hot spot from CGC image. Both images show a 2 mm diameter source at a distance of 47 mm from the CGC camera face. Scale shown is in object space, the image is larger than the source due to the resolution of the pinhole at this distance.

4 Measurements and results

4.1 Imaging phantoms

A number of different phantoms were used to provide a variety of shapes and configurations to explore the imaging response of the CGC system.

2014 JINST 9 C12020

Thyroid phantom. For thyroid simulations a Picker Nuclear thyroid phantom (Part # 3602) was used. This phantom has a total volume of 35 ml; the left hand lobe has a depth of 18.4 mm and the right hand a depth of 9.2 mm. The phantom also contains nodules, three of which were cold spots where no activity was present, and one of which was a hot spot with a depth of 18.4 mm in the 9.2 mm lobe. The phantom is sealed with a 5 mm Perspex cap. The area of the entire phantom is 60 mm^2, approximately 50% larger than a typical patient thyroid.

The phantom was filled with ^{99m}Tc from a stock solution to an activity of 100 MBq. The phantom was placed 100 mm below the camera (fitted with the 0.5 mm diameter pinhole) and a 60000 frame image accumulated ($\sim$ 30 minutes acquisition time). Figure 4 shows a schematic of the Picker phantom (l.h.s.) and an example gamma-ray image (r.h.s.). The 12 mm nodes, both hot and cold spots, are clearly distinguishable, as is the 9 mm cold spot on the low activity side of the phantom. The smallest cold spot (top left hand side) can be identified although with a much lower contrast-to-noise ratio.

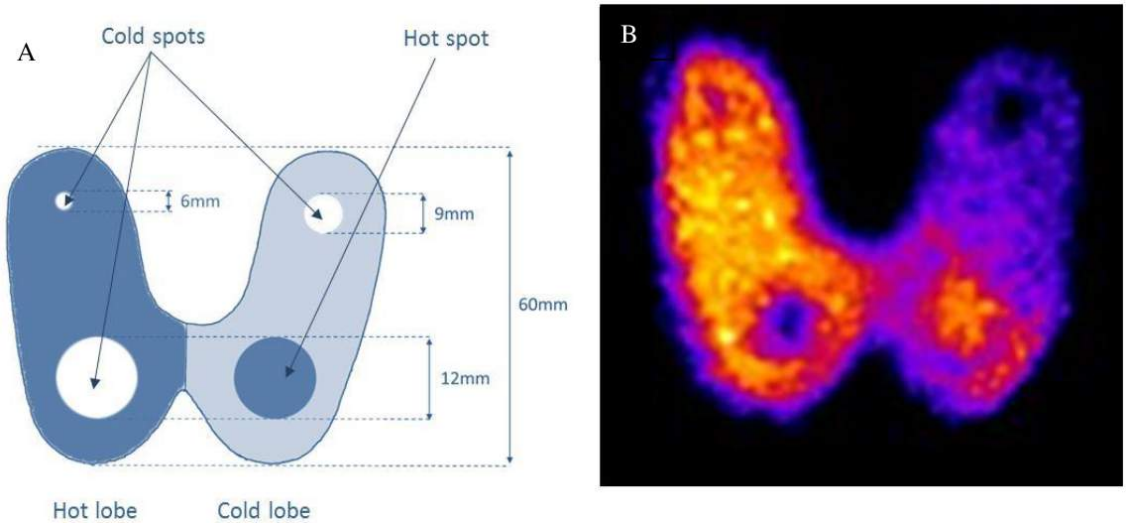

Figure 4. Left: schematic of Picker thyroid phantom. White indicates cold spots, light blue half depth and dark blue is full depth. Right: gamma image of the phantom filled with 300 MBq of ^{99m}Tc at a distance of 100 mm from 0.5 mm CGC pinhole. ($\sim$ 30 min exposure).

The long exposure image, shown in figure 4, allowed us to explore the stability and contrast-to-noise ratio of the CGC. To gauge the response and detectability of the system, a sequence of shorter exposure images was accumulated. Figure 5 shows the time sequence with exposure times ranging from 200–2000 s. As expected, the clarity of the phantom image improves with exposure time. Ultimately the choice of exposure time will rest with the clinician and will vary depending on the application and activity of the site under investigation.

Lymph node phantoms. A lymphoscintigraphic phantom has been constructed to assess the capability of the CGC for lymphatic vessel drainage imaging. In this phantom, lymphatic vessels were simulated with a 0.55 mm internal diameter cannula (0.2 MBq/mm of ^{99m}Tc) and an injection site simulated using a 10 mm maximal diameter Eppendorf tube (60 MBq of ^{99m}Tc). Varying thicknesses of Perspex, placed between the phantom and camera, were used to simulate differing

2014 JINST 9 C12020

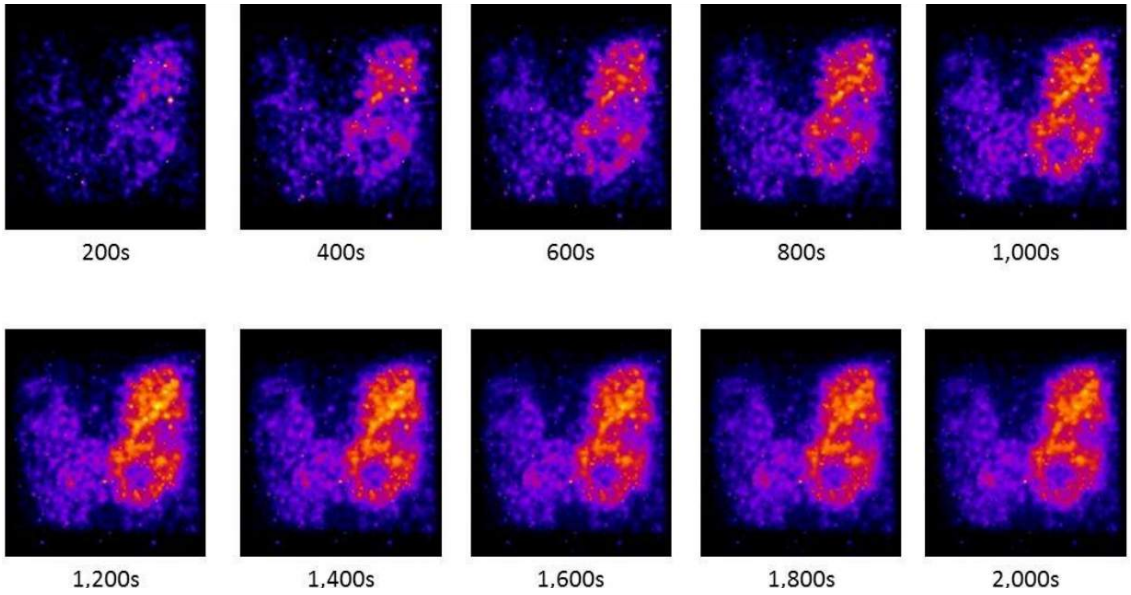

Figure 5. A time series of thyroid phantom images showing image clarity improving with increased accumulation time. The phantom contained 300 MBq of ^{99m}Tc and was placed at a distance of 160 mm from the CGC, using a 0.5 mm pinhole. The exposure time is given for each image.

depths of vessel within the body. The same phantom was also imaged using a conventional Large Field of View (LFOV) camera (Mediso Nucline X-Ring-C).

Fused optical and gamma images of the simulated lymphatic vessel produced by the CGC (figure 6) show good alignment of the two modalities — allowing accurate localisation of activity within the field of view.

In figure 7, the simulated injection site is within the FOV. Even in the presence of the high-activity injection site, the targeted lymphatic vessel can still be seen after an acquisition time of ~ 2 minutes. Increasing the exposure time to 10 minutes improves the contrast of the image (figure 7A).

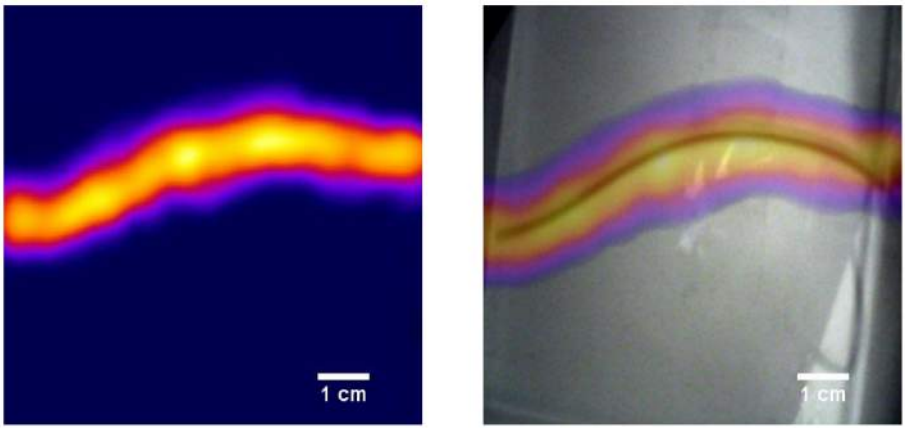

Figure 6. Gamma (l.h.s.) and hybrid (r.h.s.) images for the lymphatic vessel phantom. Image taken over $\sim$10 mins (5000 frames) at a 5 mm Perspex depth.

2014 JINST 9 C12020

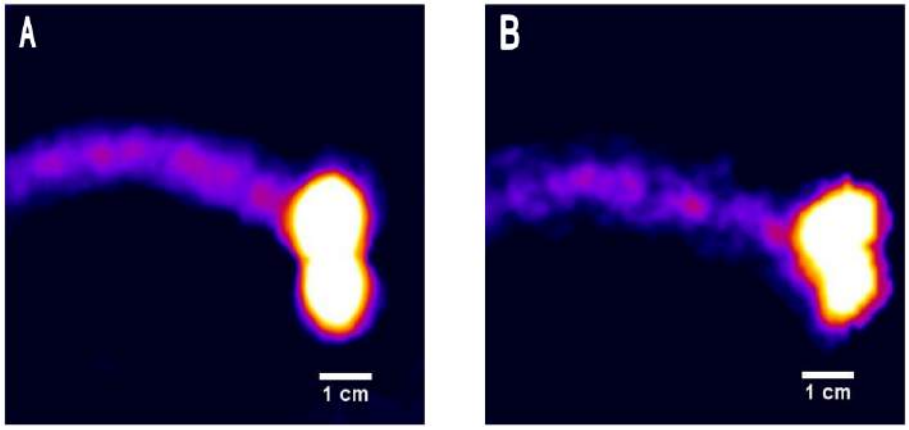

Figure 7. Gamma images showing the lymphatic vessel phantom, including the dual injection site, for two different acquisition periods. (A) has an acquisition time of $\sim$ 10 mins (5000 frames) and (B) of $\sim$ 2 mins (1000 frames). The lymphatic vessel was placed underneath 5 mm thick Perspex, with the injection site on the surface of the Perspex.

Figure 8 shows the relationship between the measured full width half maximum (FWHM) of the lymphatic vessel image and the distance from the injection site for both the CGC and the LFOV camera. The measured FWHM was significantly smaller for the CGC than the LFOV camera regardless of separation or depth of Perspex. When the distance from the centre of the modelled injection site was greater than approximately 15 mm the FWHM of the lymphatic vessel reached a constant level (variation $< 5\%$), which reflects the fundamental spatial resolution of each camera (measured at 100 mm from the source).

4.2 Imaging patients

It is anticipated that the combination of a portable gamma camera with an optical camera will have practical benefits for a number of procedures. The most obvious benefit is due to the registration of the gamma image onto the anatomical optical image, allowing the clinician to make a better assessment of radiopharmaceutical localisation during surgery leading to a more accurate diagnosis. As part of the development of the CGC, patients who were undergoing clinical investigations at the nuclear medicine clinic at Queen's Medical Centre, Nottingham were imaged with the hybrid camera following their standard clinical test as permitted following ethical approval.

Lacrimal drainage. A nuclear lacrimal drainage scan is a non-invasive study that uses a low radiation dose introduced to the eye to assess the performance of the nasolacrimal drainage system (tear duct). This procedure can be important for pre-operative planning — to determine the position of an obstruction — and post-operatively for surgical evaluation [1, 14].

Figure 9 shows a recent CGC image of a patient undergoing a lacrimal drainage investigation. 1 MBq of ^{99m}Tc-pertechnetate in a saline solution was introduced to each eye.

The gamma image is a summation of 2000 frames overlaid onto an optical image of the patient using the fusion software described in section 2. Figure 9 clearly shows good agreement between the expected location of the activity and that determined by the anatomical image.

2014 JINST 9 C12020

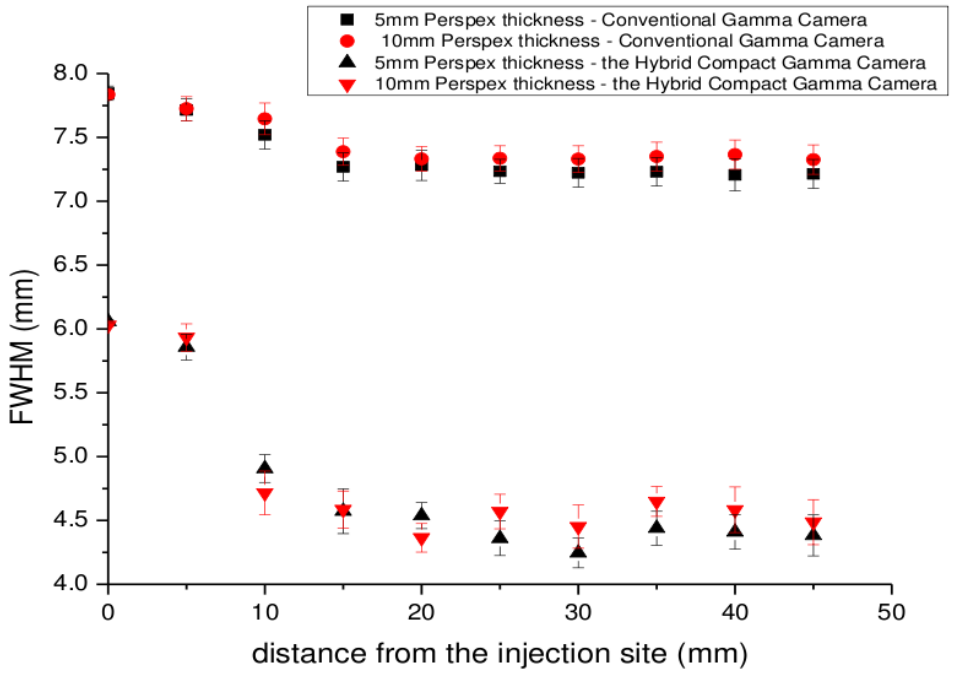

Figure 8. Comparison of the FWHM of the lymphatic phantom (injection site and lymphatic vessel) as a function of distance from the centre of the injection site for the CGC and a conventional LFOV gamma camera. Squares and circles: conventional gamma camera with 5 and 10 mm of Perspex. Triangles: CGC with 5 and 10 mm of Perspex. The imaging distance for both cameras was 100 mm.

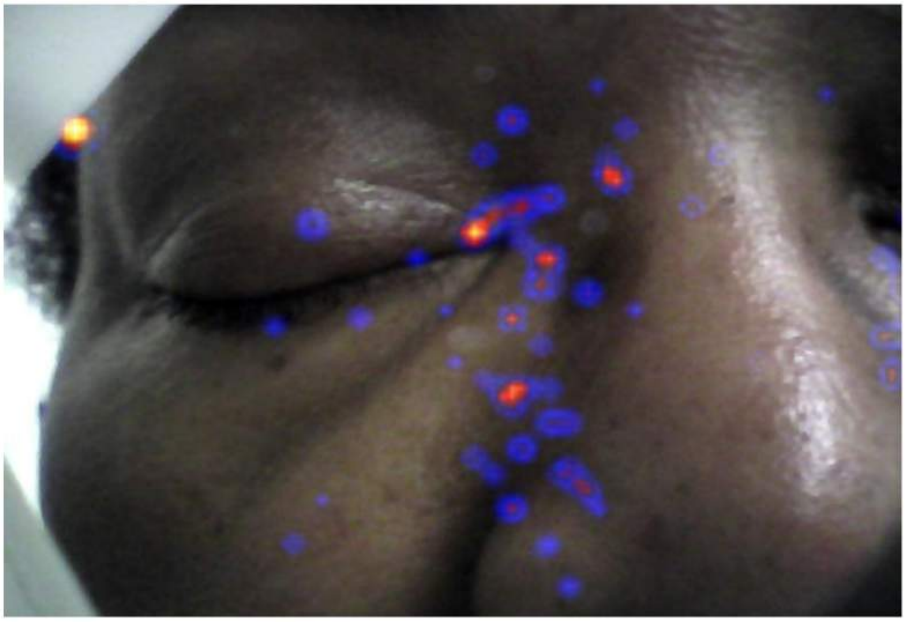

Figure 9. Composite optical and gamma image of a patient undergoing a lacrimal drainage investigation. Drainage of activity through the nasolacrimal drainage system can be clearly seen.

5 Conclusions

Intra-operative imaging is used widely in medicine, and the use of gamma camera imaging has the potential to further improve surgical outcomes. The concept of sentinel lymph node biopsy has been applied to assist in the identification of patients for complete lymph node dissection [15, 16] and has become an important technique for staging cancer and, in particular, determining whether the disease has spread from the primary tumour to the lymphatic system. This procedure is becoming standard, and is carried out over 2 million times annually. For this procedure to be successful it is necessary to identify the sentinel node pre-operatively.

The clinical advantages of fusing the gamma image to the optical image are clear and should be especially beneficial for use during surgical procedures. The CGC may have many practical benefits for a number of clinical procedures including diagnosis, surgical investigation and the visualisation of drug delivery.

We anticipate that by providing the surgeon with an overlaid image during an operation confidence in localisation of sites of uptake can be increased, reducing the procedure time and providing both a better diagnosis and outcome.

The CGC has been shown to be capable of high resolution gamma imaging combined with optical imaging to produce fused images offering improvements in a number of nuclear medicine applications. The camera has been used to produce dual-modality images from phantom simulations and patients undergoing clinical examinations.

The CGC offers combined optical and gamma imaging that will facilitate new techniques to address both existing and emerging healthcare needs, especially point-of-care and intraoperative imaging.

Acknowledgments

The authors would like to thank the late Prof. George Fraser, Space Research Centre, University of Leicester for his scientific advice. In addition we would like to thank the staff at the Leicester Royal Infirmary for their support and advice, especially David Monk and Helen Hill. The authors acknowledge the support of Science and Technologies Facilities Council through a CLASP award (ST/I003274/1).

References

[1] J. Duch. *Portable gamma cameras: the real value of an additional view in the operating theatre*, *Eur. J. Nucl. Med. Mol. Imaging* **38** (2011) 633.

[2] J.E. Lees, D.J. Bassford, O.E. Blake, P.E. Blackshaw and A.C. Perkins, *A high resolution Small Field Of View (SFOV) gamma camera: a columnar scintillator coated CCD imager for medical applications*, 2011 *JINST* **6** C12033.

[3] M. Tsuchimochi and K. Hayama, *Intraoperative gamma cameras for radioguided surgery: Technical characteristics, performance parameters, and clinical applications*, *Phys. Med.* **29** (2013) 126.

[4] S. Pitre et al., *A hand-held imaging probe for radio-guided surgery: physical performance and preliminary clinical experience*, *Eur. J. Nucl. Med. Mol. Imaging* **30** (2003) 339.

2014 JINST 9 C12020

[5] A. Ferretti et al., *Phantom study of a new hand-held gamma-imaging probe for radio-guided surgery*, *Nucl. Med. Commun.* **34** (2013) 86.

[6] C. Trotta et al., *New high spatial resolution portable camera in medical imaging*, *Nucl. Instrum. Meth.* **A 577** (2007) 604.

[7] W. Siman and S.C. Kappadath, *Performance characteristics of a new pixelated portable gamma camera*, *Med. Phys.* **39** (2012) 3435.

[8] P. Russo et al., *Evaluation of a CdTe semiconductor based compact gamma camera for sentinel lymph node imaging*, *Med. Phys.* **38** (2011) 1547.

[9] P.D. Olcott et al., *Performance Characterization of a Miniature, High Sensitivity Gamma Ray Camera*, *IEEE Trans. Nucl. Sci.* **54** (2007) 1492.

[10] A. Abe et al., *Performance evaluation of a hand-held, semiconductor (CdZnTe)-based gamma camera*, *Eur. J. Nucl. Med. Mol. Imaging* **30** (2003) 805.

[11] e2v Technologies Ltd, 106 Waterhouse Lane, Chelmsford, Essex, CM1 2QU, U.K.

[12] Hamamatsu Photonics UK Limited, 2 Howard Court, 10 Tewin Road, Welwyn Garden City, Hertfordshire, AL7 1BW, U.K.

[13] Ultimate Metals, 46 Larkshall Road, Chingford, London, E4 7HZ, U.K.

[14] A. MacDonald and S. Burrell, *Infrequently performed studies in nuclear medicine: Part 1*, *J. Nucl. Med. Technol.* **36** (2008) 132.

[15] S. Salvador et al., *Sentinel node imaging via lymphoscintigraphy*, 2007 *JINST* **2** P07003.

[16] H.S. Koops et al., *Sentinal node biopsy as a surgical staging method for solid cancers*, *Radiother. Oncol.*, **51** (1999) 1.

2014 JINST 9 C12020